Proceedings of the
Annual Stability Conference
Structural Stability Research Council
Denver, Colorado, March 22-25 2022

Analytical buckling solutions for three-member space frames subjected to torsional loading

Mani Khezri[1], Yang Hu[2], Kim J.R. Rasmussen[3]

Abstract
Torsional loading of members and its destabilizing effects are prevalent in mechanical and aerospace engineering applications where slender members are utilized to transfer significant torques. In structural engineering, the problem of buckling under torsion can be investigated at both member and frame level. While analytical solutions and numerical estimations have been derived for members, little attention has been paid to the buckling of space frames subjected to torsional loading. The purpose of this paper is to develop exact analytical buckling solutions for symmetric three-member frames subjected to torques at the supports. Frames subjected to such torsional loads can undergo large out-of-plane displacements when the exerted torques exceed the torsional buckling capacity of the structure. The developed solutions are concise and, due to their modal structure, provide new insights into the complex buckling behavior of structural frames, as well as equations to determine their slenderness and strength.

1. Introduction

In the structural engineering field, buckling is usually sought to be avoided as it is considered a marker for onset of failure. However, in recent years, a new approach has emerged in which the buckling of slender elements is exploited for novel modes of functionality (Reis (2015)). For instance, a structure with more than one stable state due to snap-through buckling is a promising solution as it can be utilized to construct functional bi-stable mechanisms (Zirbel et al. (2016)). In this rapidly evolving field, the intrinsic features of buckling, including high-rate motion, sudden energy release, and multiple equilibrium states, are viewed as assets that can be beneficially applied in designing smart and passively intelligent devices. Buckling induced applications have already been integrated into various structures with different scales (Restrepo et al. (2015), Ren et al. (2018), and Jenett et al. (2017)).

Following this line of thought, designers have been studying the buckling and post-buckling behavior of slender structural elements to find suitable mechanisms that can be employed as drivers for desired functions. Khezri et al. (2021) and Hu et al. (2021a) revisited the stability

[1] Lecturer, The University of Sydney, <mani.khezri@sydney.edu.au>
[2] PhD Candidate, The University of Sydney, <yang.hu@sydney.edu.au>
[3] Professor, The University of Sydney, <kim.rasmussen@sydney.edu.au>

problems of bars, plates and frames to identify configurations of these elements suitable for application in adaptive façade systems. They utilized the buckling of plates with retractable point-supports (Khezri et al. (2021)) to create ventilation control modules with binary (closed and open) states. Further, Hu et al. (2021) showed that the flexural-torsional buckling of slender frames has a great potential to be used for novel solutions in kinetic façades, including shading modules. Frames subjected to torsional loads at supports can be designed to undergo large out-of-plane displacements when the exerted torques exceed the torsional buckling capacity of the frame. Developing such solutions requires a thorough understanding of the buckling behaviour of slender elements and efficient tools to calculate their buckling loads for a wide range of configurations, to provide insight into how model parameters, i.e. geometric and material properties, influence the system's response. Analytical buckling solutions, because of their computational efficiency, modal nature, and reliability, are suitable tools to procure the required insight and knowledge base.

While the buckling of frames and arches subjected to in-plane and out-of-plane loadings has been extensively researched (Trahair (1993)), the buckling of frames under applied torque at supports has received little attention. This is due to the fact that structural frames are mainly subjected to gravitational and lateral forces and the loading case of torsion at supports rarely occurs in conventional structures. However, in the new paradigm of harnessing buckling for structural and morphing applications, new loading conditions are examined to achieve desired functions, including the torsional buckling of members and frames. With the motivation to better understand torsional mechanics and to use the flexural-torsional buckling of frames with end torques as driver for shading modules, this study derives analytical buckling solutions for three-member space frames subjected to torques at the supports. The symmetric three-member frame undergoes large out-of-plane displacements when subjected to the combined actions of flexural-torsional buckling and bending, and the pronounced resultant deflections can be configured for effective shading. A brief review of the existing developments on this subject is presented in the following.

While torsion rarely is the primary action causing instability in structural frames, the destabilizing effects of torsion are recognized in mechanical and aerospace engineering applications where often slender members transfer significant torques. Hence, mechanical engineers are familiar with the buckling of circular shafts that experience excessive torsion and remedy the problem by using rotary bearings along the span to decrease the free-standing length of the shaft (Trahair and Teh (2001)). The buckling of shafts with circular cross-section subjected to concentrated end torques and axial compression has been analysed by Timoshenko and Gere (1961), Ziegler (1968), and Bazant and Cedolin (1991). Yang and Kuo (1991) were the first to determine the buckling load of frames subjected to torsional loading. They analysed the stability of an angled two-member frame with one fixed support and one free end under torque action, see Fig. 1(a). The nodal torsional loadings were treated as semi-tangential (ST) (Fig. 1(b)) and quasi-tangential (QT) (Fig. 1(b)) type moments, distinguished by the different moment increments they generate about different axes. The exact solutions for various torsional loadings and three distinct cross-sections were provided as benchmarks for validating numerical analyses and design purposes. Their results showed that the critical buckling load of an angled frame is dependent on the type of torque applied at the free end. Recently, Yang and Liu (2020) extended their analytical approach to obtain exact solutions for the lateral buckling of cantilevered circular

arches subjected to various torsional moments at the free end. A comprehensive review of the works conducted by Yang and co-workers on the nonlinear analysis of framed structures and curved beams considering joint equilibrium in deformed state is available in Yang et al. (2020).

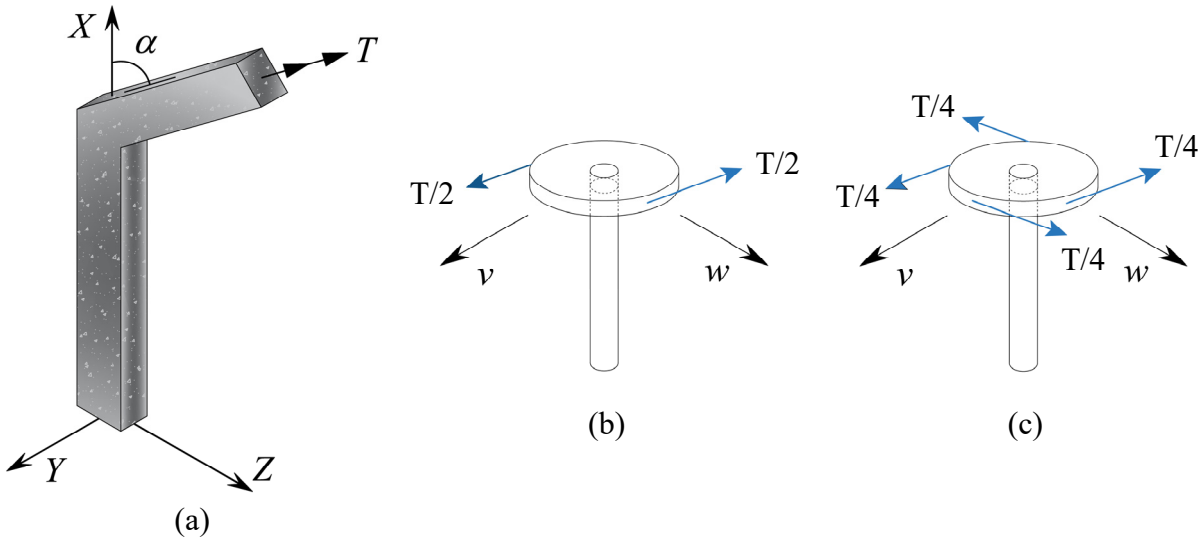

Figure 1: (a) two-member frame with one fixed support and one free end subjected to torque action, (b) semi-tangential, and (c) quasi-tangential conservative torques

To extend current knowledge and provide useful design tools, this study derives analytical buckling solutions for symmetric three-member frames subjected to torques at the supports. The derived solutions are validated using finite element analysis. The paper is structured as follows: In Section 2, the general problem of buckling of a three-member space frame subjected to end-torsional moments is stated. The governing differential equations and corresponding general solutions and internal actions for beams under bending and/or torque are provided in Sections 2.1 and 2.2. In Section 3, the analytical framework and methodology for calculating the buckling coefficients and mode shapes of symmetric three-member frames are presented. This is followed by a series of examples and numerical validations with finite-element (FE) solutions obtained using Abaqus. Section 5 concludes the paper and summarizes the main outcomes.

2. Buckling analysis of single-beam and frames subjected to end-torsional moments

The frames consist of beam elements that resist forces and moment (twisting and bending) under applied loads and undergo three-dimensional (3D) displacements and rotations. It is assumed that the deformations of the beam elements in their longitudinal directions are negligible and therefore not included in the proposed relations. The cross-sections of the beams are solid, and so the associated warping displacements are negligible and ignored in the formulation. In the following, the governing differential equations, general solutions and internal actions are presented for the following two load cases:

1. Beam elements subjected to bending only, and
2. Beam elements subjected to combined in-plane bending and torque.

2.1 Governing equations

Consider a beam element under the loading conditions shown in Fig. 2. For an infinitesimal element of the beam, dx, parallel to yz-plane at coordinate x, the governing differential equations are as follows (Yang 1989):

$$EI_z v'''' + \bar{M}_x w''' = 0, \tag{1}$$

$$EI_y w'''' - \bar{M}_x v''' + \bar{M}_z \theta'' = 0, \tag{2}$$

$$-GJ\theta'' + \bar{M}_z w'' = 0. \tag{3}$$

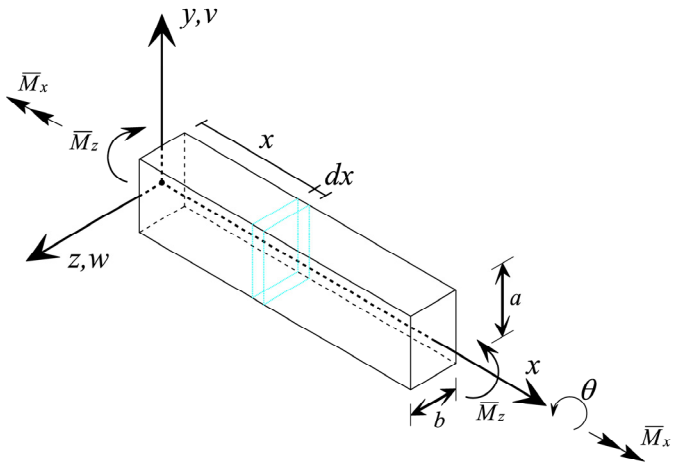

Figure 2: (a) two-member frame with one fixed support and one free end subjected to torque action, (b) semi-tangential, and (c) quasi-tangential conservative torques

In Eqs. (1) to (3), $\bar{M}_x$ and $\bar{M}_z$ are the external torque and out-of-plane bending moment at incipient buckling, which are calculated using a linear pre-buckling analysis. Each prime (′) denotes one order of differentiation with respect to the longitudinal coordinate (x). Also, v and w are the translational displacements caused by buckling in the direction of the adopted local y and z axes, and θ is the twist angle about the x-axis. E is Young's modulus, and G is the shear modulus. I_y and I_z are the second moments of area of the section about the y- and z-axes, respectively, and J is the Saint-Venant torsion constant.

2.2 General solutions

2.2.1 Members subjected to combined in-plane bending and torque

Consider member i subjected to both out-of-plane bending $\bar{M}_{z,i}$ and torque $\bar{M}_{x,i}$. The general solutions for v, w and θ obtained by solving Eqs. (1) to (3) are as follows:

$$v_i(x_i) = \left(\frac{\mu_i}{\phi_i} \left(a_i \cos\left(\frac{\phi_i x_i}{L_i} \right) - b_i \sin\left(\frac{\phi_i x_i}{L_i} \right) \right) + f_i + g_i \left(\frac{x_i}{L_i} \right) + h_i \left(\frac{x_i}{L_i} \right)^2 + e_i \frac{\lambda_i \bar{M}_{z,i}}{3\bar{M}_{x,i}} \left(\frac{x_i}{L_i} \right)^3 \right) \cdot L_i, \tag{4}$$

$$w_i(x_i) = \left(\left(a_i \sin\left(\frac{\phi_i x_i}{L_i} \right) + b_i \cos\left(\frac{\phi_i x_i}{L_i} \right) \right) + c_i + d_i \left(\frac{x_i}{L_i} \right) + e_i \left(\frac{x_i}{L_i} \right)^2 \right) \cdot L_i, \tag{5}$$

$$\theta_i(x_i) = \lambda_i \left(a_i \sin\left(\frac{\phi_i x_i}{L_i} \right) + b_i \cos\left(\frac{\phi_i x_i}{L_i} \right) + e_i \left(\frac{x_i}{L_i} \right)^2 \right) + i_i + j_i \left(\frac{x_i}{L_i} \right), \tag{6}$$

in which a_i, b_i, …, j_i are constants and,

$$\phi_i = \sqrt{\frac{EI_z\bar{M}_{z,i}^2 + GJ\bar{M}_{x,i}^2}{E^2 I_z I_y GJ}} L_i, \quad \mu_i = \frac{\bar{M}_{x,i} L_i}{EI_z}, \text{ and } \lambda_i = \frac{\bar{M}_{z,i} L_i}{GJ}. \tag{7}$$

2.2.2 Members subjected to out-of-plane bending only

For members subjected to only out-of-plane bending $\bar{M}_{z,i}$, the torque $\bar{M}_{x,i}$ is set to zero in Eqs. (4) to (6), and the general solutions for the resultant equations simplify to:

$$v_i(x_i) = \left(f_i + g_i\left(\frac{x_i}{L_i}\right) + h_i\left(\frac{x_i}{L_i}\right)^2 + e_i\left(\frac{x_i}{L_i}\right)^3 \right) \cdot L_i, \tag{8}$$

$$w_i(x_i) = \left(\left(a_i \sin\left(\frac{\eta_i x_i}{L_i}\right) + b_i \cos\left(\frac{\eta_i x_i}{L_i}\right) \right) + c_i + d_i\left(\frac{x_i}{L_i}\right) \right) \cdot L_i, \tag{9}$$

$$\theta_i(x_i) = \lambda_i \left(a_i \sin\left(\frac{\eta_i x_i}{L_i}\right) + b_i \cos\left(\frac{\eta_i x_i}{L_i}\right) \right) + i_i + j_i\left(\frac{x_i}{L_i}\right), \tag{10}$$

where η_i is deducted from ϕ_i by setting $\bar{M}_{x,i} = 0$:

$$\eta_i = \frac{\bar{M}_{z,i} L_i}{\sqrt{GJ \cdot EI_y}}. \tag{11}$$

2.3 Internal actions

Using the general solutions provided, the internal actions in the buckled configuration at location x are obtained by enforcing the equilibrium conditions for the infinitesimal element dx, see Fig. 2, as follows:

$$F_{y,i}(x_i) = -EI_z v_i'''(x_i) - \bar{M}_{x,i} w_i''(x_i), \tag{12}$$

$$F_{z,i}(x_i) = -EI_y w_i'''(x_i) + \bar{M}_{x,i} v_i''(x_i) - \bar{M}_{z,i} \theta_i'(x_i), \tag{13}$$

$$M_{y,i}(x_i) = -EI_y w_i''(x_i) + \bar{M}_{x,i} v_i'(x_i) - \bar{M}_{z,i} \theta_i(x_i), \tag{14}$$

$$M_{z,i}(x_i) = EI_z v_i''(x_i) + \bar{M}_{x,i} w_i'(x_i), \tag{15}$$

$$M_{x,i}(x_i) = GJ\theta_i'(x_i) - \bar{M}_{z,i} w_i'(x_i). \tag{16}$$

3. Analytical buckling solutions

3.1 Problem Statement

The three-member frame herein considered is shown in Fig. 3, including the torsional moments applied at the supports. Note that the moments are applied in directions causing symmetric pre-buckling displacements with respect to the global *XZ*-plane through the centerline of the frame. For the boundary conditions, other than allowing twist rotations, the supports at points A and D

are assumed to be built-in. In this study, the semi-tangential torque (Fig. 1(b)) is selected as it is comparable with concentrated torques in FE simulations.

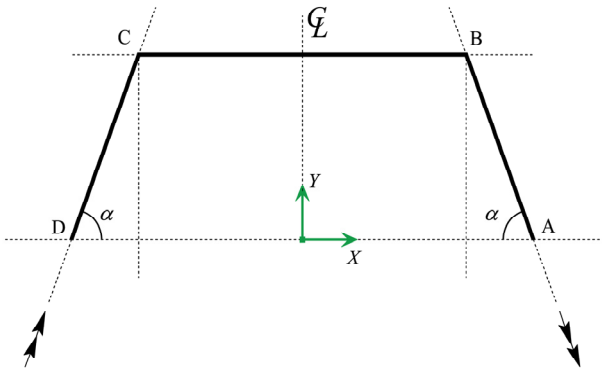

Figure 3. Considered three-member frame problem

Fig. 1(c) illustrates the semi-tangential torque which is generated by two force couples spaced a unity distance apart. This type of torque generates moment increments $Tv'/2$ and $Tw'/2$ about the y-axis and z-axis, respectively (Ziegler (1967), Yang and McGuire (1986)). The joint experiencing this type of torque satisfies the following natural boundary conditions when the bending rotational DOFs are unrestrained:

$$-EI_y w_i''(x_i) + \frac{\bar{M}_{x,i}}{2} v_i'(x_i) = 0, \tag{17}$$

$$EI_z v_i''(x_i) + \frac{\bar{M}_{x,i}}{2} w_i'(x_i) = 0. \tag{18}$$

Using Eqs. (17) and (18), the boundary conditions for a built-in member i, constrained at support j with longitudinal coordinate x_i^j are summarized in Table 1. It is noted that the twist degree of freedom (θ) is not constrained at the "built-in" supports, whereas the rate of twist (θ') is.

Table 1. Boundary condition equations of two considered support types.

Support Type	**Built-in**
Boundary Conditions	$v_i(x_i^j) = 0$
	$w_i(x_i^j) = 0$
	$\frac{d}{dx} v_i(x_i^j) = 0$
	$\frac{d}{dx} w_i(x_i^j) = 0$
	$\frac{d}{dx} \theta_i(x_i^j) = 0$

3.2 Space frame with three members

In this section, a three-member frame subjected to end torques at supports *A* and *D* is considered (see Fig. 4.). All three members have the same rectangular cross-section with dimensions $a \times b$. Supports at A and D are built in with conditions detailed in Table 1. The local coordinate systems for the members are shown in Fig. 4. The *x*-axes are aligned with the longitudinal axes of the beam, the *y*-axes are perpendicular to the global *XY* plane, and *z*-axes are positioned following the right-hand rule. As the structure is indeterminate, first, the pre-buckling distribution of moments and forces must be determined for the entire frame. The stiffness method with compatible beam elements is employed for this purpose. The pre-buckling moments and shears obtained from this analysis are substituted into the general buckling solutions for (v, w, θ) and utilised in forming the boundary and continuity conditions for the buckling analysis. The critical buckling coefficients are determined by substituting the general solution stated in Section 2.2 into the boundary conditions at A and D, and the continuity equations at joints B and C.

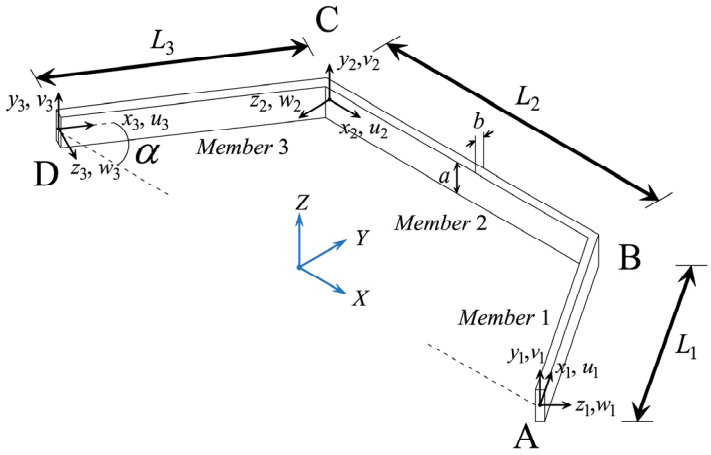

Figure 4. Schematic diagram of a three-beam frame subjected to end torques

3.2.1 General solutions for three-member angled frame

The ratio of the length of member 2 (L_2) to the length of member 1 (L_1=L) and 3 (L_3=L) is denoted by β, i.e. $\beta = L_2/L$. The results of the conducted pre-buckling analysis are presented in Fig. 5. As can be seen, the pre-buckling moments in three members are $\bar{M}_{x,1}=T$, $\bar{M}_{x,3}=-T$, $\bar{M}_{z,1}=\bar{M}_{z,3}=T\cdot\cot(\alpha)$, $\bar{M}_{z,2}=T/\sin(\alpha)$ and $\bar{M}_{x,2}=0$. Having obtained the pre-buckling stress state, and noting that the twisting moment in the central member is zero ($\bar{M}_{x,2}=0$), the general solutions for members 1, 2, and 3 can be derived by substituting the corresponding actions into Eqs. (4) to (6) (members 1 and 3) and Eqs. (8) to (10) (member 2). The general solutions for members i = 1, and 3 are given as:

$$v_i(x_i)=\left(\frac{\mu_i}{\phi_i}\left(a_i\cos\left(\frac{\phi_i x_i}{L}\right)-b_i\sin\left(\frac{\phi_i x_i}{L}\right)\right)+f_i+g_i\left(\frac{x_i}{L}\right)+h_i\left(\frac{x_i}{L}\right)^2+e_i\frac{\lambda_i\cot(\alpha)}{3}\left(\frac{x_i}{L}\right)^3\right)\cdot L, \quad (19)$$

$$w_i(x_i)=\left(\left(a_i\sin\left(\frac{\phi_i x_i}{L}\right)+b_i\cos\left(\frac{\phi_i x_i}{L}\right)\right)+c_i+d_i\left(\frac{x_i}{L}\right)+e_i\left(\frac{x_i}{L}\right)^2\right)\cdot L, \quad (20)$$

$$\theta_i(x_i)=\lambda_i\left(a_i\sin\left(\frac{\phi_i x_i}{L}\right)+b_i\cos\left(\frac{\phi_i x_i}{L}\right)+e_i\left(\frac{x_i}{L}\right)^2\right)+i_i+j_i\left(\frac{x_i}{L}\right), \tag{21}$$

in which

$$\phi_1=\phi_2=\sqrt{\frac{EI_zT^2\cot^2(\alpha)+GJT^2}{E^2I_zI_yGJ}}L,\quad \mu_1=-\mu_2=\frac{TL}{EI_z},\ \text{and}\ \lambda_1=\lambda_2=\frac{TL\cot(\alpha)}{GJ}. \tag{22}$$

Similarly, the general solutions for member 2 are obtained as:

$$v_2(x_2)=\left(f_2+g_2\left(\frac{x_2}{L_2}\right)+h_2\left(\frac{x_2}{L_2}\right)^2+e_2\left(\frac{x_2}{L_2}\right)^3\right)\cdot L_2, \tag{23}$$

$$w_2(x_2)=\left(\left(a_2\sin\left(\frac{\eta x_2}{L_2}\right)+b_2\cos\left(\frac{\eta x_2}{L_2}\right)\right)+c_2+d_2\left(\frac{x_2}{L_2}\right)\right)\cdot L_2, \tag{24}$$

$$\theta_2(x_2)=\lambda_2\left(a_2\sin\left(\frac{\eta x_2}{L_2}\right)+b_2\cos\left(\frac{\eta_2 x_2}{L_2}\right)\right)+i_2+j_2\left(\frac{x_2}{L_2}\right), \tag{25}$$

where

$$\eta=\frac{TL_2}{\sqrt{GJ\cdot EI_y}\sin(\alpha)},\ \text{and}\ \lambda_2=\frac{TL_2}{GJ\sin(\alpha)}. \tag{26}$$

The equations for each member have ten integration constants, and hence the total number of unknowns in the equations equals 30. As it will be discussed later, the axial force of member 2 appears in the developed equations and will be treated as an additional independent unknown. In summary, the matrix collects the coefficients for 31 unknown.

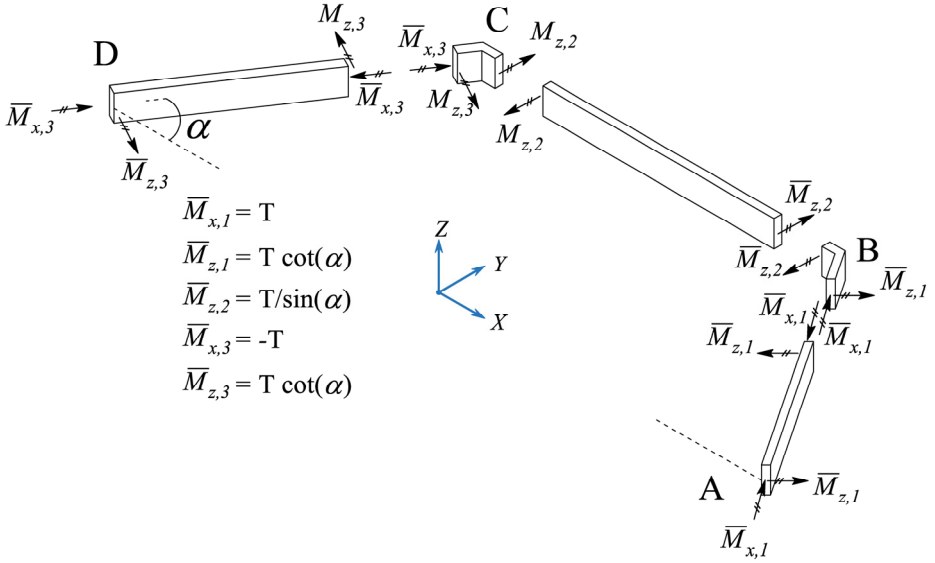

Figure 5. Schematic diagram showing the pre-buckling moments for a three-member frame

3.2.2 Support boundary conditions for three-member angled frame

The boundary conditions for the considered three-member frame are derived by substitution of the member number and local coordinates in the equations stated in Table 1. The five boundary conditions for support *A* and support *D* are determined by substituting $x_1^A = 0$ and $x_3^D = 0$, yielding in total ten equations. These equations are concisely presented in Table 2.

Table 2: Built-in boundary conditions at the supports of a three-member angled frame

Built-in BC	**Support A**		**Support D**	
$v_i(0)=0$	$\frac{(\mu_1 a_1 + f_1\phi_1)L}{\phi_1} = 0$	(27)	$\frac{(\mu_3 a_3 + f_3\phi_3)L}{\phi_3} = 0$	(28)
$w_i(0)=0$	$(b_1 + c_1)\cdot L = 0$	(29)	$(b_3 + c_3)\cdot L = 0$	(30)
$\frac{d}{dx}v_i(0)=0$	$-\mu_1 b_1 + g_1 = 0$	(31)	$-\mu_3 b_3 + g_3 = 0$	(32)
$\frac{d}{dx}w_i(0)=0$	$\phi_1 a_1 + d_1 = 0$	(33)	$\phi_3 a_3 + d_3 = 0$	(34)
$\frac{d}{dx}\theta_i(0)=0$	$\frac{\cot(\alpha)TL\cdot\phi_1\cdot a_1 + GJ\cdot j_1}{GJ\cdot L} = 0$	(35)	$\frac{\cot(\alpha)TL\cdot\phi_3\cdot a_3 + GJ\cdot j_3}{GJ\cdot L} = 0$	(36)

Further equations can be derived by imposing the compatibility of the displacements at joints B and C. Four equations are obtained by utilizing simple geometric relations between the displacements in the deformed configuration as shown in Fig. 6, viz.

$$v_1(L) = v_2(\beta L), \tag{37}$$

$$v_3(L) = v_2(0), \tag{38}$$

$$\cos(\alpha) w_1(L) = -w_2(\beta L), \tag{39}$$

$$\cos(\alpha) w_3(L) = w_2(0). \tag{40}$$

The assumption of negligible axial displacement for member 2 (i.e. $u_2(0) = u_2(\beta L)$) implies that the transverse displacements of members 1 and 2 must be the same, viz.

$$w_1(L) = w_3(L). \tag{41}$$

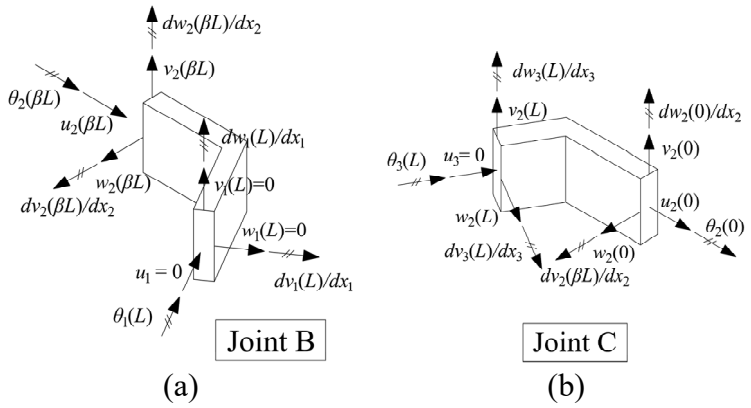

Figure 6. Schematic diagram of displacements, slopes and twist rotations at (a) Joint *B* and; (b) Joint *C*

The internal actions induced in the members during buckling are shown in Fig. 7. Considering joint *B* (see Fig. 7(c)), the equilibrium equations of forces and moment are,

$$F_{y,1}(L) = -F_{y,2}(\beta L), \tag{42}$$

$$F_{z,1}(L) = -\sin(\alpha) F_{x,2} + \cos(\alpha) F_{z,2}(\beta L), \tag{43}$$

$$M_{y,1}(L) = -M_{y,2}(\beta L), \tag{44}$$

$$M_{z,1}(L) = -\sin(\alpha) M_{x,2}(\beta L) + \cos(\alpha) M_{z,2}(\beta L), \tag{45}$$

$$M_{x,1}(L) = \sin(\alpha) M_{z,2}(\beta L) + \cos(\alpha) M_{x,2}(\beta L), \tag{46}$$

where $F_{x,2}$ is unknown. Likewise, for joint *C* (see Fig. 7(e)), the equilibrium conditions are

$$F_{y,3}(L) = F_{y,2}(0), \tag{47}$$

$$F_{z,3}(L) = \sin(\alpha) F_{x,2} + \cos(\alpha) F_{z,2}(0), \tag{48}$$

$$M_{y,3}(L) = M_{y,2}(0), \tag{49}$$

$$M_{z,3}(L) = \sin(\alpha) M_{x,2}(0) + \cos(\alpha) M_{z,2}(0), \tag{50}$$

$$M_{x,3}(L) = -\sin(\alpha) M_{z,2}(0) + \cos(\alpha) M_{x,2}(0). \tag{51}$$

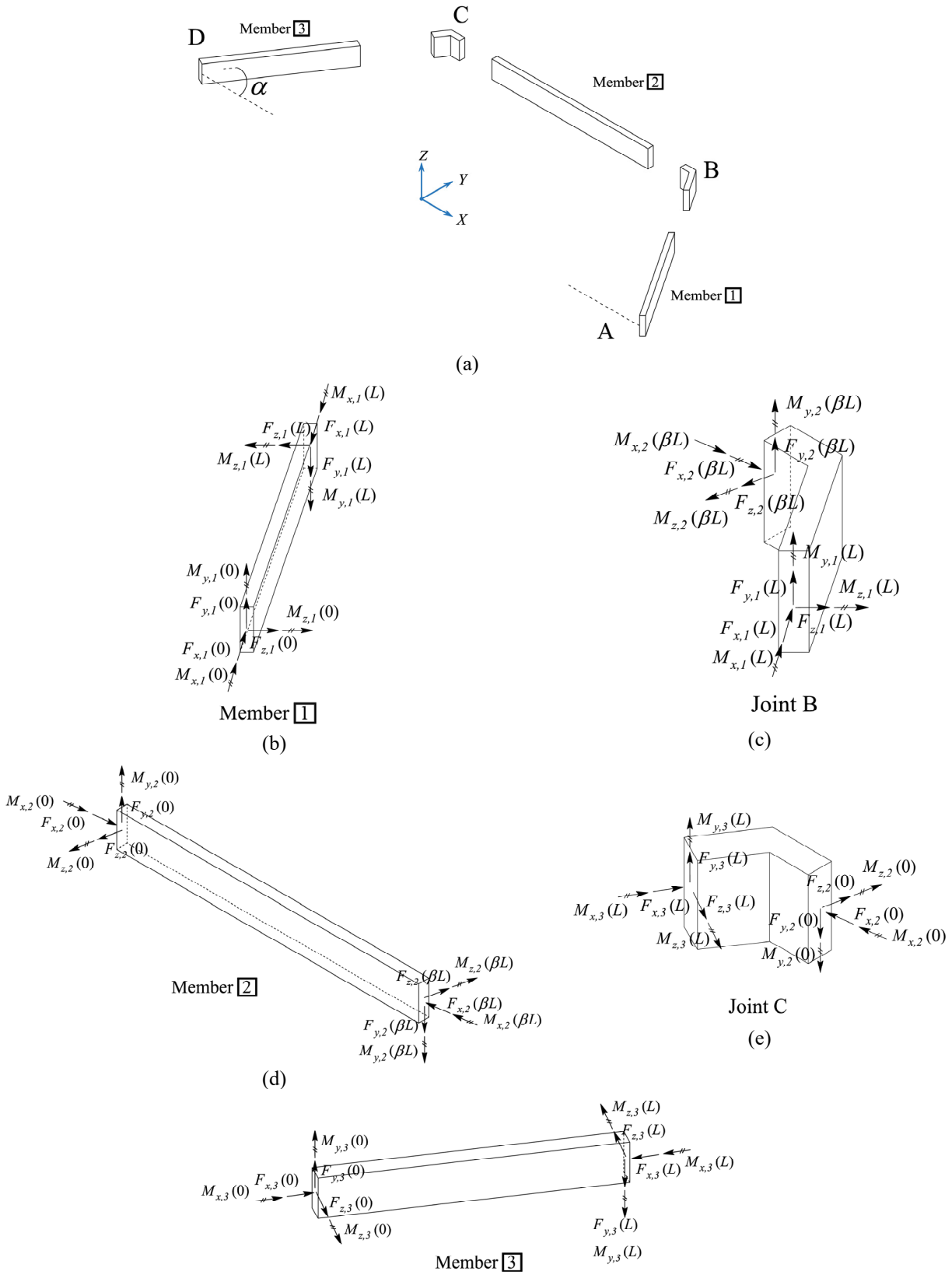

Figure 7. Schematic diagram of the forces and moments for each member and each joint of a three-member frame

Thus far, we have obtained 25 equations. The remaining equations are derived by enforcing the slope continuity conditions at joints *B* and *C* (see Fig. 6). For joint *B*, we have:

$$\frac{d}{dx}w_1(L)=\frac{d}{dx}w_2(\beta L), \tag{52}$$

$$\frac{d}{dx}v_1(L)=\sin(\alpha)\cdot\theta_2(\beta L)-\cos(\alpha)\cdot\frac{d}{dx}v_2(\beta L), \tag{53}$$

$$\frac{d}{dx}v_2(\beta L)=-\sin(\alpha)\cdot\theta_1(L)-\cos(\alpha)\cdot\frac{d}{dx}v_1(L), \tag{54}$$

and similarly, for joint *C* the equations are:

$$\frac{d}{dx}w_3(L)=\frac{d}{dx}w_2(0), \tag{55}$$

$$\frac{d}{dx}v_3(L)=\sin(\alpha)\cdot\theta_2(0)+\cos(\alpha)\cdot\frac{d}{dx}v_2(0), \tag{56}$$

$$\frac{d}{dx}v_2(0)=-\sin(\alpha)\cdot\theta_3(L)+\cos(\alpha)\cdot\frac{d}{dx}v_3(L). \tag{57}$$

By substituting the internal actions given in Eqs. (12) to (16) and general solutions into Eqs. (37) to (57), the following equations can be obtained in terms of the integration constants considering $\mu_1 = -\mu_3 = \mu$ and $\phi_1 = \phi_3 = \phi$:

$$\frac{\mu}{\phi}\left(\cos(\phi)a_1-\sin(\phi)b_1\right)+\frac{\lambda_1\cot(\alpha)}{3}e_1+\left(f_1+g_1+h_1\right)-\left(e_2+f_2+g_2+h_2\right)\beta=0, \tag{58}$$

$$-\frac{\mu}{\phi}\left(\cos(\phi)a_3-\sin(\phi)b_3\right)-\frac{\lambda_3\cot(\alpha)}{3}e_3+\left(f_3+g_3+h_3\right)-\beta f_2=0, \tag{59}$$

$$\left(\sin(\phi)a_1+\cos(\phi)b_1+c_1+d_1+e_1\right)\cos(\alpha)+\beta\left(\sin(\eta)a_2+\cos(\eta)b_2+c_2+d_2\right)=0, \tag{60}$$

$$\left(\sin(\phi)a_3+\cos(\phi)b_3+c_3+d_3+e_3\right)\cos(\alpha)-\beta\left(b_2+c_2\right)=0, \tag{61}$$

$$\left(a_1-a_3\right)\sin(\phi)+\left(b_1-b_3\right)\cos(\phi)+\left(c_1-c_3\right)+\left(d_1-d_3\right)+\left(e_1-e_3\right)=0, \tag{62}$$

$$\frac{2\left(EI_z\lambda_1\cos(\alpha)+TL\sin(\alpha)\right)}{\sin(\alpha)}e_1+\frac{6EI_z}{\beta^2}e_2=0, \tag{63}$$

$$\frac{-2\beta Th_1+T\left(\beta j_1-j_2\right)\cot(\alpha)-\beta L\sin(\alpha)F_{x2}}{\beta L}=0, \tag{64}$$

$$\left(-2EI_y e_1/L+\left(g_1+2h_1\right)T\right)-T\cot(\alpha)\left(i_1+j_1\right)-T\csc(\alpha)\left(i_2+j_2\right)=0, \tag{65}$$

$$\frac{T\beta L\left(d_1-d_2\right)+2\beta\left(TL+EI_z\cot\left(\alpha\right)\lambda_1\right)e_1+2EI_z\left(\beta h_1-\left(3e_2+h_2\right)\cos\left(\alpha\right)\right)+GJ\sin\left(\alpha\right)j_2}{\beta L}=0, \quad (66)$$

$$\frac{GJ\beta j_1-\cot\left(\alpha\right)\left(T\beta L\left(d_1-d_2\right)+GJ\sin\left(\alpha\right)j_2\right)-2EI_z\sin\left(\alpha\right)\left(3e_2+h_2\right)}{\beta L}=0, \quad (67)$$

$$\frac{2\left(EI_z\lambda_3\cos\left(\alpha\right)+TL\sin\left(\alpha\right)\right)}{\sin\left(\alpha\right)}e_3+\frac{6EI_z}{\beta^2}e_2=0, \quad (68)$$

$$\frac{2\beta Th_3+T\left(\beta j_3-j_2\right)\cot\left(\alpha\right)+\beta L\sin\left(\alpha\right)F_{x2}}{\beta L}=0, \quad (69)$$

$$-\left(2EI_ye_3/L+\left(g_3+2h_3\right)T\right)-T\cot\left(\alpha\right)\left(i_3+j_3\right)+T\csc\left(\alpha\right)i_2=0, \quad (70)$$

$$\frac{-T\beta L\left(d_3-d_2\right)-2\beta\left(TL+\lambda_3EI_z\cot\left(\alpha\right)\right)e_3+2EI_z\beta h_3-2EI_z\cos\left(\alpha\right)h_2-GJ\sin\left(\alpha\right)j_2}{\beta L}=0, \quad (71)$$

$$\frac{GJ\beta j_3-\cot\left(\alpha\right)\left(T\beta L\left(d_3-d_2\right)+GJ\sin\left(\alpha\right)j_2\right)+2EI_z\sin\left(\alpha\right)h_2}{\beta L}=0, \quad (72)$$

$$-\phi\left(\cos\left(\phi\right)a_1-\sin\left(\phi\right)b_1\right)-d_1-2e_1+\eta\left(\cos\left(\eta\right)a_2-\sin\left(\eta\right)b_2\right)+d_2=0, \quad (73)$$

$$\begin{aligned}&-\left(\left(\sin\left(\eta\right)a_2+\cos\left(\eta\right)b_2\right)\lambda_2-\left(3e_2+g_2+2h_2\right)\cot\left(\alpha\right)+i_2+j_2\right)\sin\left(\alpha\right)\\&-\left(\mu\left(\sin\left(\phi\right)a_1+\cos\left(\phi\right)b_1\right)-\cot\left(\alpha\right)\lambda_1e_1-g_1-2h_1\right)=0,\end{aligned} \quad (74)$$

$$\left(\begin{matrix}\left(\lambda_1-\mu\cot\left(\alpha\right)\right)\left(\sin\left(\phi\right)a_1+\cos\left(\phi\right)b_1\right)\\+\cot\left(\alpha\right)\left(g_1+2h_1\right)+i_1+j_1\end{matrix}\right)\sin\left(\alpha\right)+\lambda_1\csc\left(\alpha\right)e_1+\left(g_2+2h_2+3e_2\right)=0, \quad (75)$$

$$-\phi\left(\cos\left(\phi\right)a_3-\sin\left(\phi\right)b_3\right)-d_3-2e_3+\eta a_2+d_2=0, \quad (76)$$

$$\left(\sin\left(\phi\right)\mu a_3+\cos\left(\phi\right)\mu b_3-\lambda_3\cot\left(\alpha\right)e_3+g_3+2h_3\right)-\left(\lambda_2b_2+i_2\right)\sin\left(\alpha\right)-\cos\left(\alpha\right)g_2=0, \quad (77)$$

$$\left(\begin{matrix}\left(\lambda_3-\mu\cot\left(\alpha\right)\right)\left(\sin\left(\phi\right)a_3+\cos\left(\phi\right)b_3\right)\\-\cot\left(\alpha\right)\left(g_3+2h_3\right)+i_3+j_3\end{matrix}\right)\sin\left(\alpha\right)+\lambda_3\csc\left(\alpha\right)e_3+g_2=0. \quad (78)$$

Having determined the BCs and continuity equations, the coefficient matrix can be formed by collecting the respective terms of the integration constants and the unknown axial force $F_{x,2}$ as follows:

$$\left[\underbrace{\begin{matrix}\mathbf{C}_1 & \mathbf{C}_2 & \mathbf{C}_3 & \mathbf{C}_4\end{matrix}}_{\mathbf{C}}\right]\left\{\begin{matrix}\hat{\mathbf{d}}_1\\\hat{\mathbf{d}}_2\\\hat{\mathbf{d}}_3\\\underbrace{F_{x2}}_{\mathbf{d}}\end{matrix}\right\}=\left\{\begin{matrix}0\\0\\\vdots\\0\end{matrix}\right\}. \quad (79)$$

The determinant of the matrix is obtained using Matlab and equated to zero to obtain the buckling loads. The complete forms of the coefficient matrix **C** (31×31) and solution vector **d** (31×1) are given in (Hu et al. 2021b) but not stated herein.

4. Example: Three-member frame subjected to torques at supports

In this section, the application of the developed buckling analysis of a symmetric three-member space frame subjected to torques at the supports is demonstrated through an example. The beam members are all placed in the global *XY*-plane, as shown in Figure 8. The frame is assumed to be symmetric with respect to the central *YZ*-plane passing through the origin of the coordinate system. Member 1 and Member 3 are positioned with angle α with respect to the global *X*-axis, while Member 2 is parallel to this axis. All members have a solid rectangular cross-section with dimensions $a \times b$. Dimension b is measured in the Z direction.

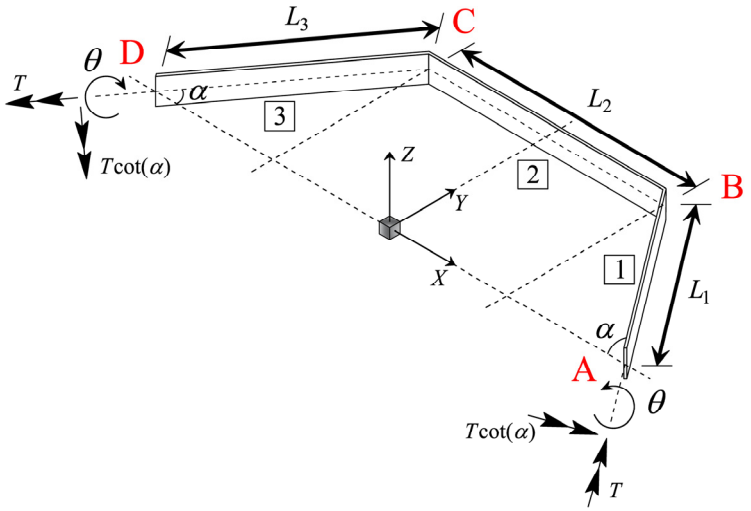

Figure 8. Schematic diagram showing the coordinate systems of a three-member frame

A series of analyses is conducted for frames with β (L_2 / L_1) ratios of 0.5, 1.0, 2.0 and 10.0. In these analyses, the aspect ratio $\zeta = b/a$ of the cross-section is equal to 1, 5, and 10, and the angle α is varied from 5° to 90°. The acquired results using the analytical method are presented in Figure 9, Figure 10, and Figure 11, corresponding to the aspect ratios ζ = 1, 5, and 10, respectively. The solutions obtained are normalized using the buckling coefficient K, defined as:

$$K = \frac{TL_1}{\pi\sqrt{EI_z EI_y}}. \tag{80}$$

The same figures compare the results with FE linear buckling solutions obtained using Abaqus, indicating that for all considered values of β, the analytical and numerical solutions are in excellent agreement.

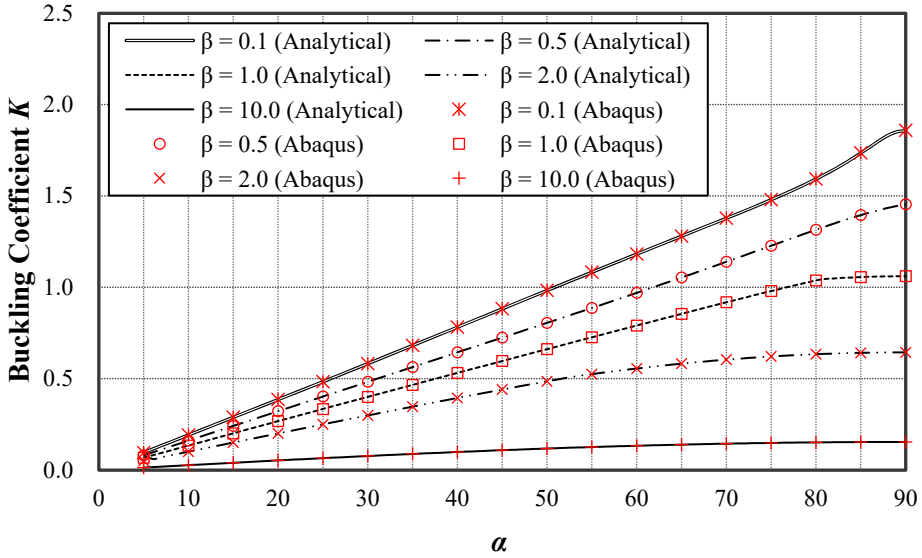

Figure 9. Comparison of buckling coefficients (K) obtained from analytical solutions and FEA for a three-member frame with aspect ratio $\zeta = 1$

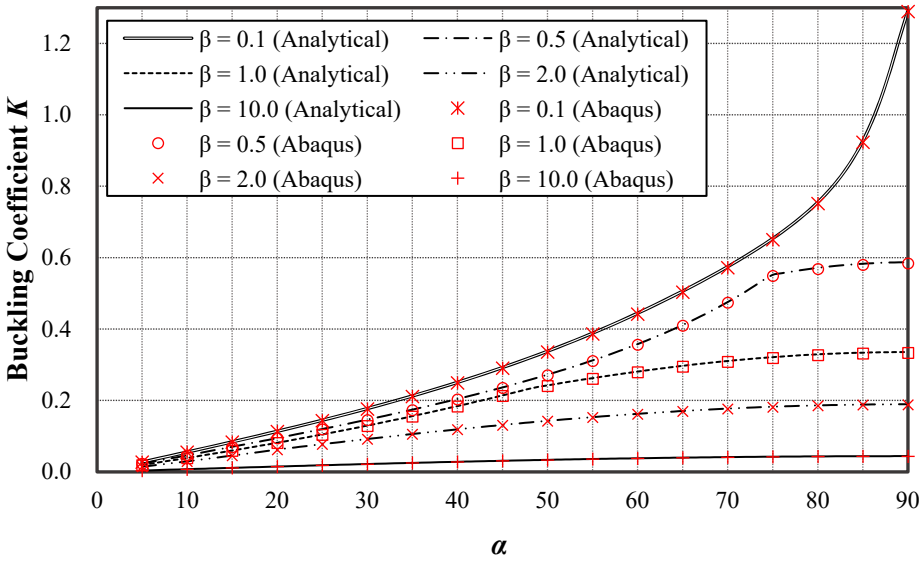

Figure 10. Comparison of buckling coefficients (K) obtained from analytical solutions and FEA for a three-member frame with aspect ratio $\zeta = 5$

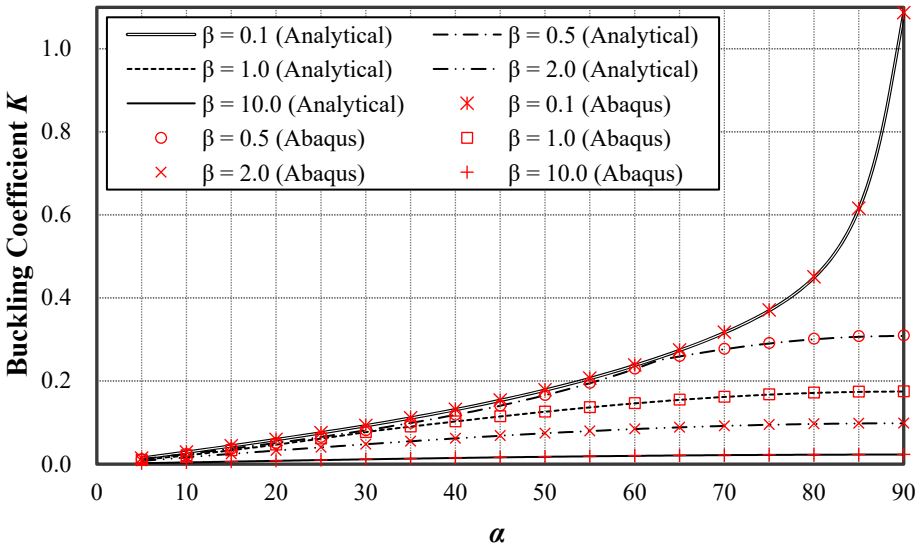

Figure 11. Comparison of buckling coefficients (K) obtained from analytical solutions and FEA for a three-member frame with aspect ratio $\zeta = 10$

It is evident from Fig. 9, Fig. 10, and Fig. 11 that frames with lower β-values (shorter relative lengths (L_2) of the central member) have higher buckling capacity. In some curves, slope discontinuities can be observed. For example, in Figure 10, the curve representing $\beta = 0.5$ shows a sudden change of slope when the angle α reaches 75°. This suggests a change in the symmetry of the buckling mode, which is further studied in the following.

Having validated the analytical solutions for specific cases of frames with different β- and α-values, the analytical method is next utilized to analyze a wide range of three-member frame problems. The three key parameters, namely α, β, and ζ, are varied over practical ranges, and solutions for the resultant combinations are obtained. The values of β vary from 0.1 to 10, and the selected values of ζ are 1, 2, 5 and 10. The possible combinations of β and ζ are analysed for specific values of α varying from 15° to 90° in 30° increments, viz. α = 15°, 45° and, 75° and 90°. The results obtained are normalized using Eq. 80 and are presented in Fig. 12, Fig. 13, and Fig. 14.

The general trend in Fig. 9 to Fig. 10 is that frames with larger α-values but same aspect ratios ζ and member length ratios β have higher buckling capacities for all the six considered modes. A close inspection of the graphs reveals that in some cases, the curves for consecutive modes, e.g. one and two, or three and four, assume the same values. For example, considering the graphs for α = 45°, ζ = 10 (Figure13(d)), the curves for modes 1 and 2 are coincident when β = 0.72, and likewise for modes 3 and 4 when β = 1.13, which implies mode shape changes at these points.

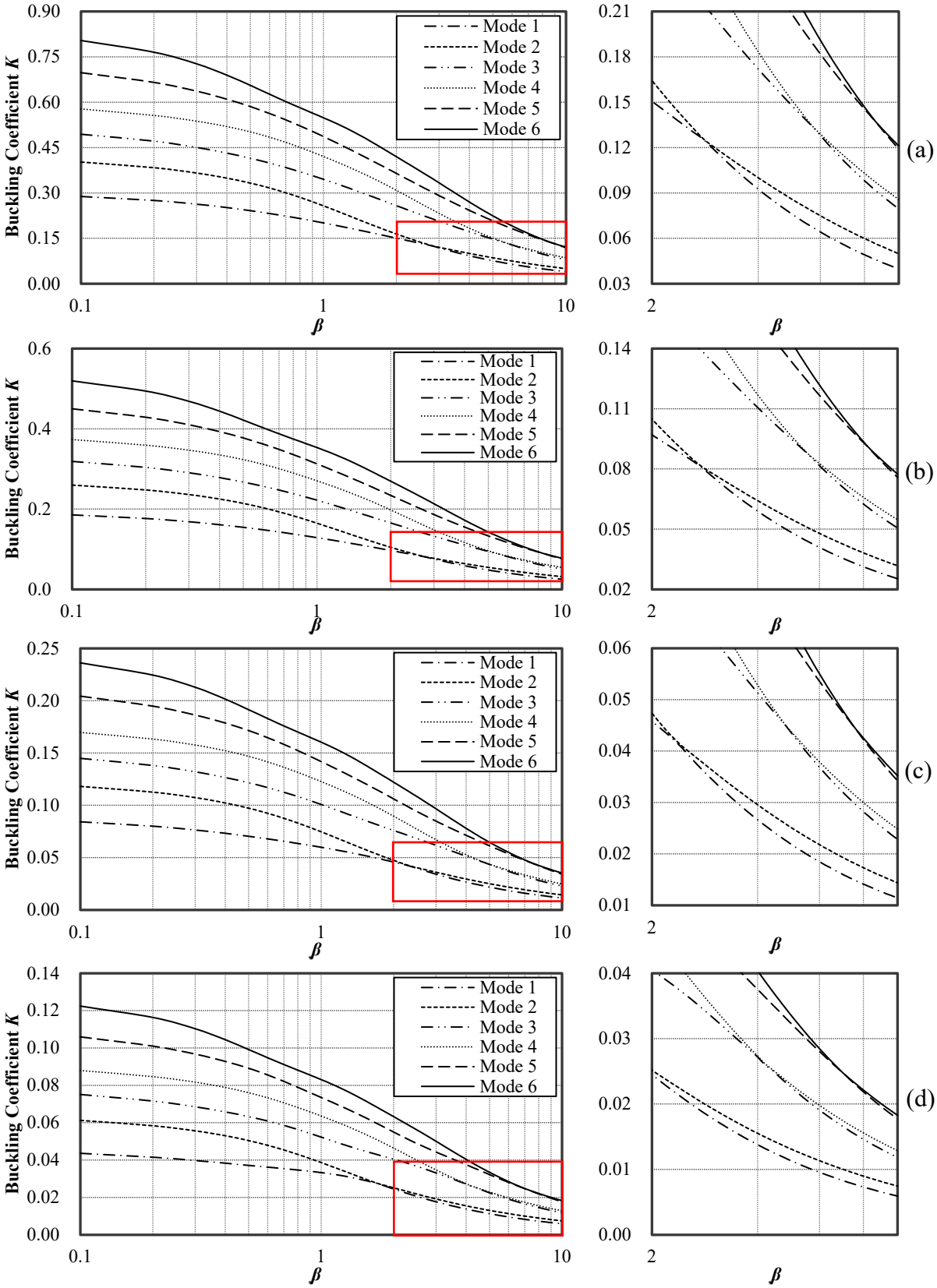

Figure 12. Buckling coefficient (K) versus β ranging from 0.1 to 10 for a three-member frame with angle $\alpha = 15°$ for aspect ratios (a) ζ=1; (b) ζ=2; (c) ζ=5; (d) ζ=10.

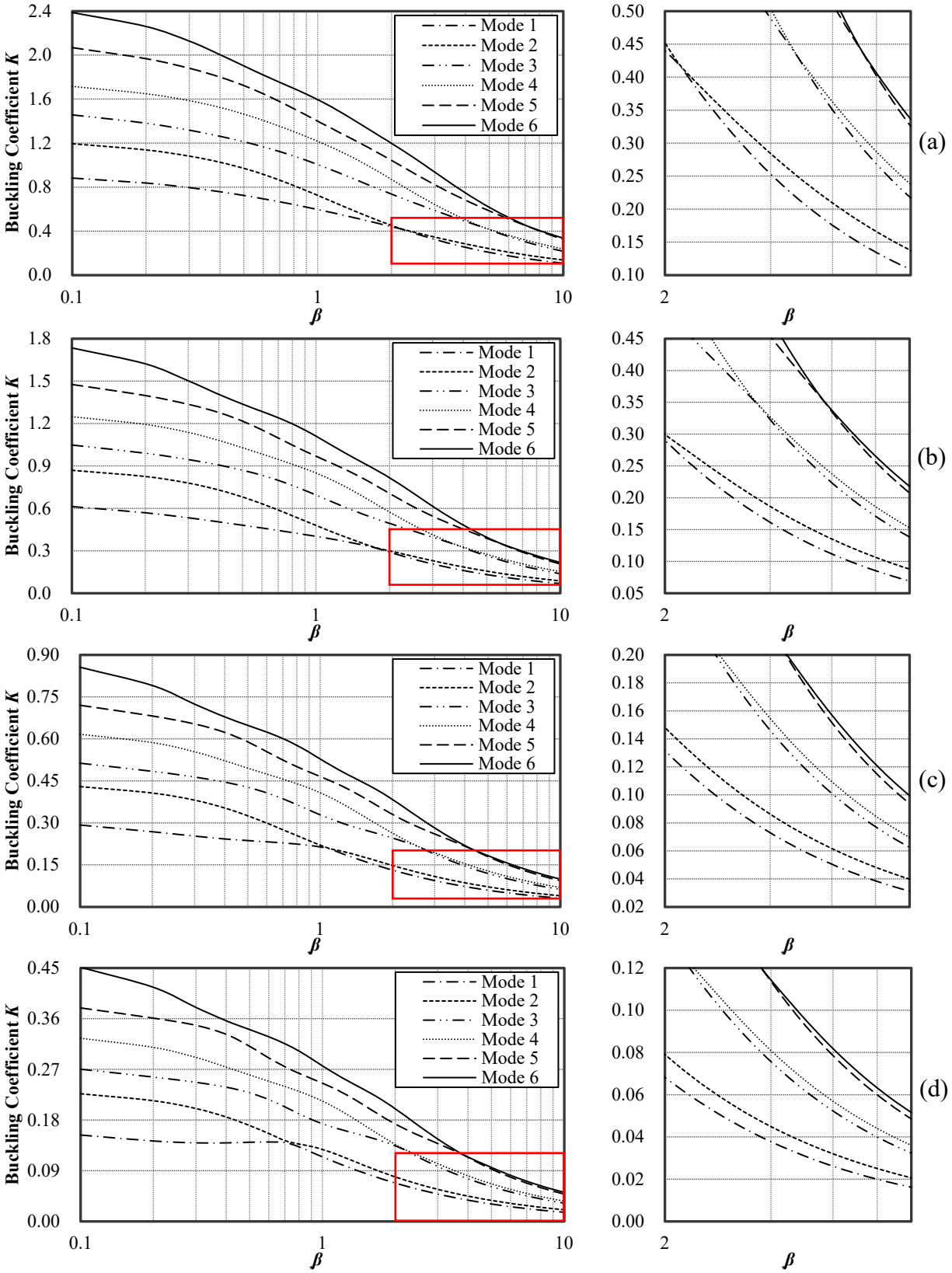

Figure 13. Buckling coefficient (K) versus β ranging from 0.1 to 10 for a three-member frame with angle $\alpha = 45°$ for aspect ratios (a) ζ=1; (b) ζ=2; (c) ζ=5; (d) ζ=10.

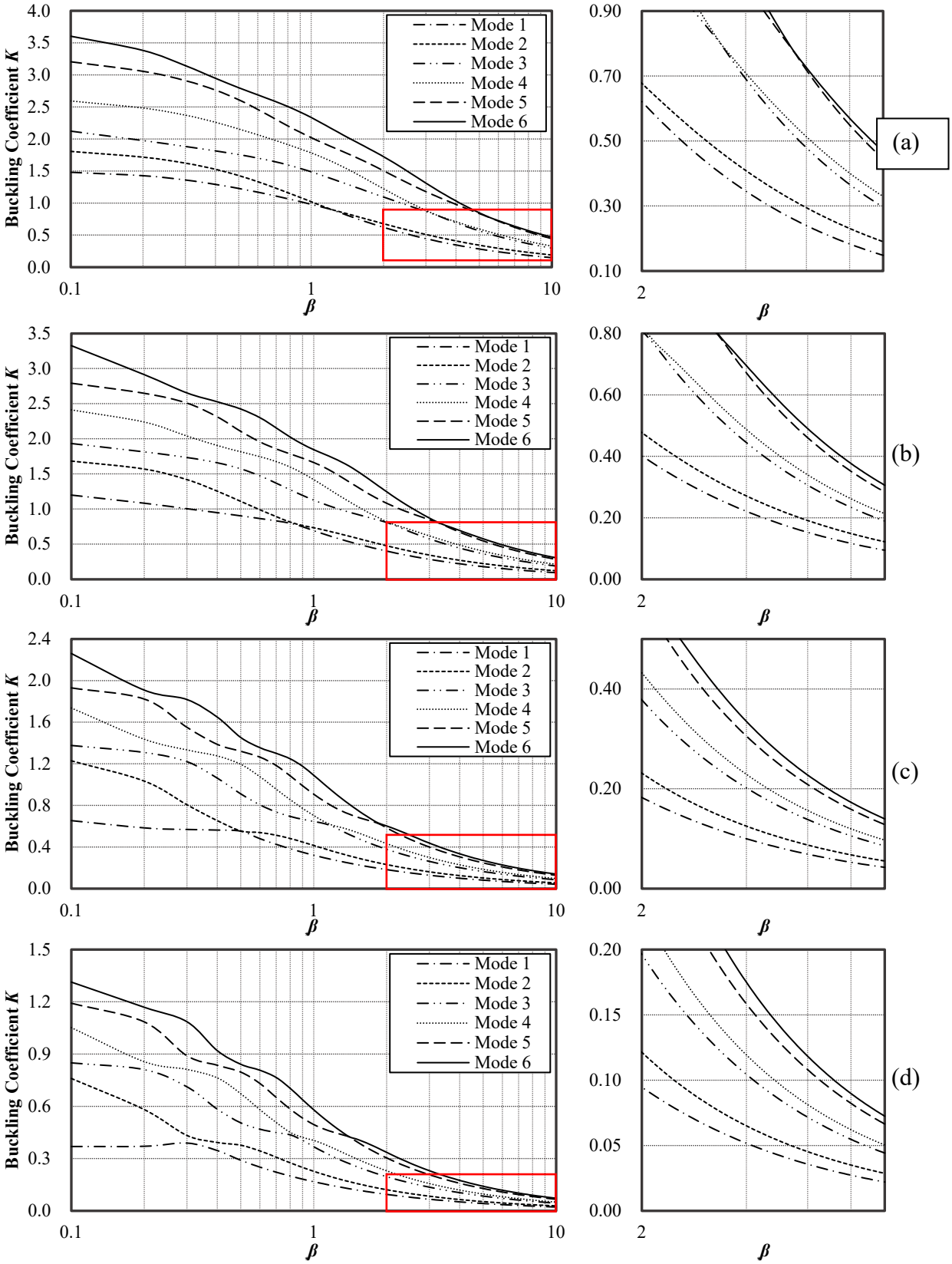

Figure 14. Buckling coefficient (K) versus β ranging from 0.1 to 10 for a three-member frame with angle $\alpha = 75°$ for aspect ratios (a) ζ=1; (b) ζ=2; (c) ζ=5; (d) ζ=10.

5. Conclusions

The paper presents analytical buckling solutions for three-member frames subjected to end torsional moments. The three-member frames are assumed to be symmetric about the centerline with members rigidly connected at angles varying between 0 and 90º. Distinctly different buckling loads are obtained depending on the angle between members and the aspect ratio of the cross-section. The solutions are obtained by solving the governing equations and as such can be considered exact. They therefore also serve as benchmarks for checking the accuracy of future numerical analyses. Throughout the study, the cross-section is assumed to be solid and warping effects are ignored.

Acknowledgments

This project was undertaken as part of the Australian Research Council (ARC) Discovery Project DP1701049.

References

Bazant Z.P., Cedolin L. (1991). "Stability of structures", Oxford University Press, New York.

Hu, Y., Khezri, M.,–Rasmussen, K.J.R. (2021a). "Numerical Simulation and Verification of Adaptive Shading Modules With Buckling as Driver for Functionality." (CIMS 2021).

Hu, Y., Khezri, M., Rasmussen, K.J.R. (2021b). " Analytical solutions for buckling of space frames subjected to torsional loadings." Research Report, The University of Sydney.

Jenett, B., Calisch, S., Cellucci, D., Cramer, N., Gershenfeld, N., & Cheung, K. C. (2017). "Digital morphing wing: active wing shaping concept using composite lattice-based cellular structures." *Soft robotics*, 4(1), 33-48.

Khezri, M., Rasmussen, K.J.R. (2021). "Shading Module With Buckling as Driver for Shape Morphing." (CIMS 2021).

Körner, A., Born, L., Mader, A., Sachse, R., Saffarian, S., Westermeier, A.S., Poppinga, S., Bischoff, M., Gresser, G.T., Milwich, M. and Speck, T. (2017). "Flectofold—a biomimetic compliant shading device for complex free form facades." *Smart Materials and Structures*, 27(1), 017001.

Lienhard, J., Schleicher, S., Poppinga, S., Masselter, T., Milwich, M., Speck, T., & Knippers, J. (2011). "Flectofin: a hingeless flapping mechanism inspired by nature." *Bioinspiration & biomimetics*, 6(4), 045001.

Reis, P.M. (2015). "A perspective on the revival of structural (in) stability with novel opportunities for function: from buckliphobia to buckliphilia." *Journal of Applied Mechanics*, 82.11: 111001.

Ren, C., Yang, D., Qin, H. (2018). "Mechanical performance of multidirectional buckling-based negative stiffness metamaterials: an analytical and numerical study." *Materials*, 11(7), 1078.

Restrepo, D., Mankame, N. D., & Zavattieri, P. D. (2015). "Phase transforming cellular materials." *Extreme Mechanics Letters*, 4, 52-60.

Zirbel, S. A., Tolman, K. A., Trease, B. P., & Howell, L. L. (2016). "Bistable mechanisms for space applications." *PloS one*, 11(12), e0168218.

Timoshenko S.P., Gere J.M. (1961). "Theory of elastic stability", McGraw-Hill, New York (1961)

Trahair N.S.(1993). "Flexural-torsional buckling of structures" CRC press

Trahair, N.S., Teh, L.H. (2001). "Second order moments in torsion members." *Engineering structures*, 23(6).

Yang, Y.B. (1989). Theory of stability for framed structures- Nonconservative systems. *In National Science Council, Proceedings*, 13, 202-210.

Yang, Y.B., Chen, A., He, S., Wu, Y.T. (2020). "Rational nonlinear analysis of framed structures and curved beams considering joint equilibrium in deformed state. " *International Journal of Non-Linear Mechanics*, 125, 103538.

Yang, Y.B., Kuo, S.R. (1991). "Buckling of frames under various torsional loadings." *Journal of engineering mechanics*, 117(8), 1681-1697.

Yang, Y.B., Liu, Y.Z. (2020). "Lateral buckling of cantilevered circular arches under various end moments." *International Journal of Structural Stability and Dynamics*, 20(07), 2071005.

Yang, Y. B., McGuire, W. (1986). "Stiffness matrix for geometric nonlinear analysis". *Journal of Structural Engineering*, 112(4), 853-877.

Ziegler, H. (1968). "Principles of Structural Stability", Blaisdell, Waltham, MA.